A 5G-NR Satellite Extension for the QuaDRiGa Channel Model

Stephan Jaeckel*, Leszek Raschkowski†, and Lars Thiele†

* SJC Wireless, Berlin, Germany, jaeckel@sjc-wireless.com

†Fraunhofer Heinrich Hertz Institute, Berlin, Germany

Abstract—Low Earth orbit (LEO) satellite networks will become an integral part of the global telecommunication infrastructure. Modeling the radio-links of these networks and their interaction with existing terrestrial systems is crucial for the design, planning and scaling of these networks. The 3rd generation partnership project (3GPP) addressed this by providing guideline for such a radio-channel model. However, the proposed model lacks a satellite orbit model and has some inconsistencies in the provided parameters. This is addressed in this paper. We provide a non-geostationary-satellite model that can be integrated into geometry-based stochastic channel models (GSCMs) such as QuaDRiGa. We then use this model to obtain the GSCM parameters from a simplified environment model and compare the results to the 3GPP parameter-set. This solves the inconsistencies, but our simplified approach does not consider many propagation effects. Future work must therefore rely on measurements or accurate Ray-tracing models to obtain the parameters.

I. Introduction

3GPP released a comprehensive study on non-terrestrial networks (NTNs) [1] in order include space or airborne vehicles into the 5G infrastructure. These offer wide service coverage capabilities and reduced vulnerability to physical attacks or natural disasters. The idea is to foster the roll-out of 5G services in unserved areas, reinforce the 5G service reliability, and enable improved network scalability. To enable simulation studies, such as link-budget analysis, link and system-level performance studies or coexistence analysis with terrestrial cellular networks, channel model guidelines have been provided. A model calibration was done in [2] for several aspects of the model. To support these activities, NTNs have been added to the QuaDRiGa channel model [3]. However, since QuaDRiGa has been developed primarily for terrestrial applications, some modifications are necessary to incorporate NTNs. On the other hand, many additional modeling components are already available that go beyond the 3GPP guidelines. This allows more complex simulations to be conducted, but requires modifications to the model:

a) Coordinate system: The 3GPP NTN model [1] uses a simplified "Earth centered Earth fixed" coordinate system, whereas the terrestrial 3GPP model [4] uses metric local Cartesian coordinates. In order to combine the two models, we provide a coordinate transformation that maps orbital positions and trajectories into the local Cartesian coordinates.

b) Frequency range: [4] includes an optional model for multiple frequencies which has been implemented in QuaDRiGa [5]. However, this option was not considered by [1]. Hence, [1] only provides model parameters for the S-band (2-4 GHz) and for the KA-band (26.5-40 GHz). We provide parameters that support a continuous frequency range from 2-40 GHz. Thus, we can use the multi-frequency option and also perform simulations at the commonly used KU-band (10.7-17.5 GHz).

c) Spatial Consistency: Another optional feature provided by [4] is spatial consistency (SC) which solves the problem of achieving realistic correlations in multi-user wireless channels. This becomes important for multi-satellite simulations where, for example, the line of sight (LOS) to multiple satellites might be blocked by the same building. SC is available in QuaDRiGa [6] and can be used for NTN channels.

d) Mobility: Satellites in low Earth orbit are highly mobile, causing large differential delays and Doppler shifts. However, none of the 3GPP models supports mobility at both ends of the link. The assumption in [1] is that all satellite positions are fixed. A dual-mobility model is available in QuaDRiGa [5], [6]. It can be used to simulate entire satellite constellations and track orbital movements for a longer time-period. This requires that the model parameters are given as a function of the satellite elevation angle.

GSCMs have of two main components: a stochastic part that generates a random propagation environment around the mobile terminal (MT) location on Earth, and a deterministic part that lets transmitters (e.g., the satellites) and receivers (the MTs) interact with this environment. The stochastic part requires model parameters to be extracted from radio channel measurements. However, in order to capture all model parameters, such measurements require specific channel sounding hardware. Channel measurements using satellites (e.g [7]) are then either limited in bandwidth, elevation angle range, and spatial resolution, or they are done with terrestrial transceivers (e.g. [8]). Another approach is to use deterministic Raytracing simulations to obtain the GSCM parameters. This has been favored by the 3GPP community. However, the simulations for [1] were done using high-altitude platforms (HAPs) and there are inconsistencies in the environments. This leads to questionable results when comparing the parameters of different environments, such as the Ricean K-Factor for the Suburban

and Rural scenarios. For this reason, we used a different approach where we generate random satellite constellations, MT positions and propagation environments. Based on these inputs, radio channel coefficients are generated in a purely deterministic way using QuaDRiGa. The data is then analyzed in the same way as measurement or Raytracing data would be. In this way, we get a complete set of consistent parameters for the stochastic model.

The paper is structured as follows: Section II introduces the satellite orbit model and the coordinate transformation procedure. Section III then combines this model with the existing radio channel model to obtain the large-scale fading (LSF) parameters. Results are discussed in Section IV. An open-source implementation is available as part of the quasi deterministic radio channel generator (QuaDRiGa) [3].

II. Non-GSO Satellite Orbit Model

a) Orbit model: The satellite orbit model [9] uses Earth's attraction as the main factor for orbital motion. Six parameters define the satellite position (see Fig. 1): 1) the length of the semi-major axis $a = \frac{R_a + R_p}{2}$; 2) the eccentricity $e = \frac{R_a - R_p}{R_a + R_p}$ determines the amount by which an orbit deviates from a circle (0 yields a circular orbit); 3) the inclination angle ι measures the tilt of the orbit; 4) the longitude of the ascending node Ω orients the point where the orbit passes upward through the equatorial plane; 5) the argument of periapsis ω defines the orientation of the ellipse in the orbital plane; and, 6) the true anomaly ν defines the position of the satellite along that ellipse. Given the values Ω_0, ω_0 and ν_0 at a reference time, orbit mechanics predict the position of the satellite in the future.

TABLE I
CONSTANTS REQUIRED FOR ORBIT PREDICTION

Parameter	Notation	Value	Unit
Radius of the Earth	R_e	6378.137	km
Mass of the Earth	M_e	$5.9722 \cdot 10^{24}$	kg
Earth' rotation period	T_e	86164.09054	s
Earth's angular rotation rate	ω_e	$7.29211585453 \cdot 10^{-5}$	rad/s
Gravitational constant	G	$6.67408 \cdot 10^{-20}$	km^3/s^2/kg
Earth's non-sphericity factor	J_2	0.001082636	-

Orbit perturbations are mainly due to Earth's oblateness. This is modeled by changing the ascending node longitude and perigee argument. For a given time point t relative to the reference time, the values $\Omega(t)$ and $\omega(t)$ are updated to

$$\Omega(t) = \Omega_0 - t \cdot \bar{n} \cdot \bar{p} \cdot \cos\iota, \tag{1}$$
$$\omega(t) = \omega_0 + t \cdot \bar{n} \cdot \bar{p} \cdot \left(2 - 2.5 \cdot \sin^2\iota\right), \tag{2}$$

where the parameters $\bar{n}$ and $\bar{p}$ are given by

$$\bar{n} = \sqrt{\frac{G \cdot M_e}{a^3}} \cdot \left(1 + \bar{p} \cdot \left(1 - 1.5 \cdot \sin^2\iota\right) \cdot \sqrt{1 - e^2}\right), \tag{3}$$

$$\bar{p} = \frac{3 \cdot J_2 \cdot R_e^2}{2a^2 \cdot (1 - e^2)^2}. \tag{4}$$

The constants M_e, R_e, G and J_2 can be found in Table I. An update of $\nu(t)$ is calculated using the eccentric anomaly $\{E_0, E(t)\}$ instead of the true anomaly $\{\nu_0, \nu(t)\}$ by solving

$$E(t) - e \cdot \sin E(t) = E_0 - e \cdot \sin E_0 + \bar{n} \cdot t, \tag{5}$$

where the transformation between E and ν follows from

$$\tan\left(\frac{E}{2}\right) = \sqrt{\frac{1 + e}{1 - e}} \cdot \tan\left(\frac{\nu}{2}\right). \tag{6}$$

With the updated parameters $\Omega(t)$, $\omega(t)$ and $\nu(t)$ it is possible to calculate the satellite position in Cartesian coordinates by

$$x_i = R \cdot \{\cos(\omega + \nu) \cdot \cos\Omega - \sin(\omega + \nu) \cdot \sin\Omega \cdot \cos\iota\} \tag{7}$$

$$y_i = R \cdot \{\cos(\omega + \nu) \cdot \sin\Omega - \sin(\omega + \nu) \cdot \cos\Omega \cdot \cos\iota\} \tag{8}$$

$$z_i = R \cdot \sin(\omega + \nu) \cdot \sin\iota, \tag{9}$$

where R is the distance between Earth's center and the satellite

$$R(t) = \frac{a \cdot (1 - e)^2}{1 + e \cdot \cos\nu(t)}. \tag{10}$$

To calculate the satellite coordinates as seen by an observer on Earth, Earth's rotation needs to be taken into account. This is done by translating the satellite positions into a geographic coordinate system and adding the Earth's angular rotation.

$$\theta_r(t) = \arctan_2\left\{z_i(t), \sqrt{x_i^2(t) + y_i^2(t)}\right\} \tag{11}$$
$$\phi_r(t) = \arctan_2\left\{y_i(t), x_i(t)\right\} - \omega_e \cdot t \tag{12}$$

$\arctan_2(y, x)$ is the four quadrant inverse tangent of the elements y and x having values between $-\pi$ and π. At the reference time $t = 0$, Earth's prime meridian is aligned with the vernal equinox. The satellite coordinates in rotating Cartesian coordinates (x_r, y_r, z_r) follow from the transformation

$$x = R \cdot \cos\phi \cdot \cos\theta, \tag{13}$$
$$y = R \cdot \sin\phi \cdot \cos\theta, \tag{14}$$
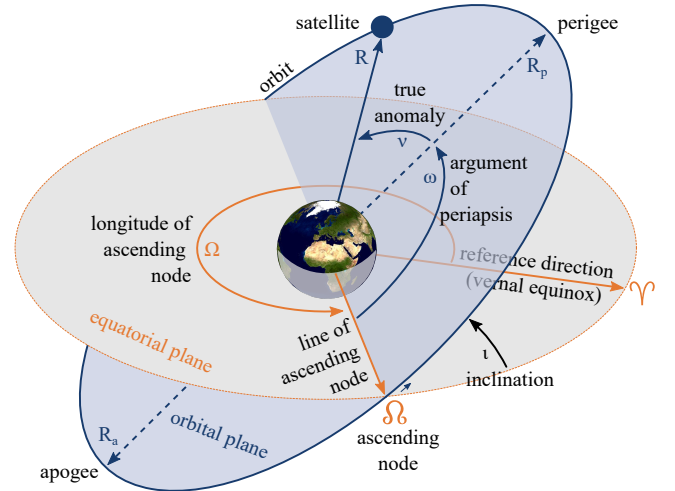$$z = R \cdot \sin\theta. \tag{15}$$

Fig. 1. Diagram illustrating various terms in relation to satellite orbits

b) Coordinate transformation: The MT-centric coordinate system is defined by a tangential plane having its origin at a reference position on Earth given by its longitude ϕ_u, latitude θ_u and radius R_e. The transformation (13)-(15) converts these to Cartesian coordinates (x_u, y_u, z_u). The transformation of the satellite coordinates (x_r, y_r, z_r) into MT-centric coordinates is done by

$$\begin{bmatrix} x_q(t) \\ y_q(t) \\ z_q(t) \end{bmatrix} = \mathbf{R}_q \cdot \begin{bmatrix} x_r(t) - x_u \\ y_r(t) - y_u \\ z_r(t) - z_u \end{bmatrix}, \quad (16)$$

where the rotation matrix $\mathbf{R}_q$ aligns the geographic Cartesian coordinate system with the MT-centric coordinate system whose x-axis points eastwards and y-axis points northwards.

$$\mathbf{R}_q = \begin{bmatrix} -\sin\phi_u & \cos\phi_u & 0 \\ -\sin\theta_u\cos\phi_u & -\sin\theta_u\sin\phi_u & \cos\theta_u \\ \cos\theta_u\cos\phi_u & \cos\theta_u\sin\phi_u & \sin\theta_u \end{bmatrix} \quad (17)$$

The satellite is visible above the horizon when $z_q(t) > 0$ and its elevation angle is

$$\alpha(t) = \arctan_2\left\{z_q(t), \sqrt{x_q^2(t) + y_q^2(t)}\right\}. \quad (18)$$

Satellites use directional antennas. Hence, the satellite's orientation towards the observer on Earth is important. The following steps calculate this orientation, assuming that the satellite is spinning at one revolution per orbit so that the same side always faces the Earth. First, three vectors are calculated

$$\mathbf{U} = \begin{bmatrix} x_u & y_u & z_u \end{bmatrix}^T, \quad (19)$$
$$\mathbf{R}(t) = \begin{bmatrix} x_r(t) & y_r(t) & z_r(t) \end{bmatrix}^T, \quad (20)$$
$$\mathbf{D}(t) = \mathbf{R}(t + \Delta t) - \mathbf{R}(t). \quad (21)$$

They are normalized to unit-length vectors $\bar{\mathbf{U}}$, $\bar{\mathbf{R}}(t)$ and $\bar{\mathbf{D}}(t)$. The vector $\bar{\mathbf{D}}(t)$ is the direction of travel calculated from two orbital positions at time points t and $t+\Delta t$. The *bank angle* β is the orientation around the axis drawn through the body of the satellite from tail to nose, relative to the tangential plane.

$$\beta_q(t) = \arcsin\left\{\bar{\mathbf{U}}^T \cdot \left(\bar{\mathbf{R}}(t) \times \bar{\mathbf{D}}(t)\right)\right\}. \quad (22)$$

The *heading angle* γ is the pointing direction of the satellite.

$$\bar{\mathbf{D}}_q(t) = \mathbf{R}_q \cdot \bar{\mathbf{D}}(t) \quad (23)$$
$$\gamma_q(t) = \arctan_2\left\{y_{\bar{\mathbf{D}}_q}(t), x_{\bar{\mathbf{D}}_q}(t)\right\} \quad (24)$$

The *tilt angle* δ is the vertical orientation of the satellite.

$$\delta_q(t) = \arctan_2\left\{z_{\bar{\mathbf{D}}_q}(t), \sqrt{x_{\bar{\mathbf{D}}_q}^2(t) + y_{\bar{\mathbf{D}}_q}^2(t)}\right\} \quad (25)$$

The six parameters $x_q, y_q, z_q, \beta_q, \gamma_q, \delta_q$ define the satellite's position and orientation as seen by an observer on Earth. Hence, satellites can be used as transmitters in GSCMs such as QuaDRiGa. Their orbital motion can be tracked over time and so can be their communication links. This enables the realistic simulation of the propagation channels of entire satellite networks.

III. OBTAINING GSCM MODEL PARAMETERS

GSCMs are parametric models, i.e. the properties of the communication links depend on the model parameters. In this section, we describe a procedure to obtain these parameters. An overview is given in Fig. 2. We created random satellite constellations using Walker-Delta patterns at three different orbit heights: 550 km, 2,000 km, and 20,200 km. The inclination angles were 53°, 61°, and 63°, respectively. Random MT positions were chosen in between ±53° latitude on Earth, assuming that the MT is outdoors at 1.5 m height above ground. The positions were imported into the QuaDRiGa channel model using the coordinate transformation from Sec. II. Then, we created a simplified random propagation environment around the MT position. The assumption is that in a satellite channel, non-line of sight (NLOS) paths must come from objects close to the MT (e.g., buildings, trees, cars, etc.). The distribution of these objects depends on the scenario. Seen from the MT, we created between 6 and 10 random arrival directions drawn from a Uniform distribution in the range $[-\pi, \pi[$. The distances to the scatterers are modeled by a truncated Gaussian distribution having a mean and standard deviation (STD) according to Table II. Truncation was done at the minimum and maximum values in Table II. Those distances reflect the building density in the environment.

A second parameter describes the height of the scatterers above the ground. This parameter reflects the typical building heights in the environment. Most scattered paths come from objects at the same height as the MT. However, high buildings in urban and dense urban settings also cause paths arriving from higher elevation angles. For the sake of simplicity, only single-bounce scattering is assumed. Multiple reflections of the signal would not change the arrival angular spread (AS) and the effect on the departure AS is negligible due to the large distance to the satellite in orbit. We further assume that each NLOS path carries on average the same amount of power. Hence, for each satellite-MT link, we can obtain a value for the NLOS path loss (PL) and shadow fading (SF) according
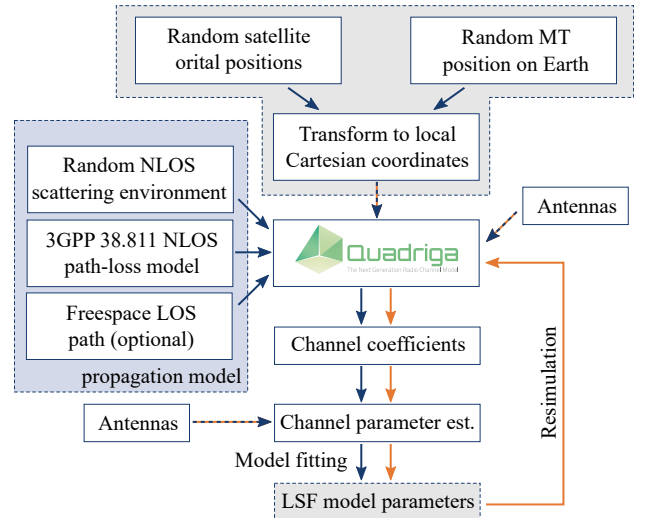

Fig. 2. Satellite LSF model parameter estimation workflow

Scenario	no. paths	Distance to scatterer (m)				Scatterer height (m)			
		min.	max.	mean	STD	min.	max.	mean	STD
Dense Urban	10	0.1	100	40	30	0	60	2	18
Urban	10	0.1	200	50	35	0	30	2	9
Suburban	8	0.1	500	65	50	0	8	1.5	1.5
Rural	6	0.1	3500	300	200	0	8	1.5	1.5

to [1] and divide this value by the number of NLOS paths in the scenario. For the LOS model, we simply add a free space path to the NLOS model. Departure and arrival direction are defined by the satellite and MT positions and the power is given by the free-space path loss (FSPL) model.

To obtain channel coefficients from QuaDRiGa, we also need antenna models for the satellite and the MT. For the satellite, we used a simple omnidirectional left hand circular polarized (LHCP) antenna. However, at the MT, we want to estimate the arrival angles from the channel coefficients. Hence, we need an array antenna with sufficient spatial resolution. This is achieved by placing 28 vertically polarized patch elements around a sphere. The distance of each element to the center of the sphere is 1.6 λ and each pair of neighboring elements is placed 1 λ apart. Side lobes are suppressed by reducing the full width at half maximum (FWHM) of the single elements to 20° . This ideal spherical array antenna has a gain of 14 dBi and a FWHM of 16° for all arrival directions. Using the algorithms from [10], it is possible to estimate the arrival direction of a path in azimuth and elevations with less than 1° error. Additional circularly polarized elements are used to calculate the cross polarization ratio (XPR).

The remaining steps of the procedure are the generation of the channel coefficients, the extraction of the channel parameters (delays, angles, delay spread (DS), ASs, K-Factor, etc.) and fitting a multilinear regression model to these parameters. The complete list of parameters consists of

- the path loss (PL) and shadow fading (SF),
- the Ricean K-factor (KF),
- the root mean square (RMS) delay spread (DS),
- the RMS azimuth spread of arrival (ASA),
- the RMS azimuth spread of departure (ASD),
- the RMS elevation spread of arrival (ESA),
- the RMS elevation spread of departure (ESD), and
- the cross polarization ratio (XPR).

The methods for extracting the channel parameters are described in [10]. The linear model for the large-scale parameters (LSPs) is given by

$$V = V_\mu + V_\epsilon \cdot \log_{10} d + V_\gamma \cdot \log_{10} f_{\text{GHz}} + V_\alpha \cdot \log_{10} \alpha_{\text{rad}} + X \left(V_\sigma + V_\delta \cdot \log_{10} f_{\text{GHz}} + V_\beta \cdot \log_{10} \alpha_{\text{rad}} \right), \quad (26)$$

where X is a Normal distributed random variables having zero-mean and unit variance. The seven parameters are: the reference value V_μ at 1 GHz, 1 m distance, and 1 rad (57.2°) elevation; the distance dependence V_ϵ of the reference value scaling with $\log_{10} d$; the frequency dependence V_γ of the reference value scaling with $\log_{10} f_{\text{GHz}}$; the elevation dependence V_α of the reference value scaling with $\log_{10} \alpha_{\text{rad}}$; the reference

STD V_σ at 1 GHz, 1 m distance, and 1 rad elevation; the frequency dependence V_δ of the reference STD scaling with $\log_{10} f_{\text{GHz}}$; and the elevation dependence V_β of the reference STD scaling with $\log_{10} \alpha_{\text{rad}}$. These parameters can be used in GSCMs to generate a randomized propagation environment for creating channel coefficients for simulation studies.

The analysis results are shown in Table III. The last step is a resimulation step where the scatterers are generated by the QuaDRiGa channel model as described in [4]. Random delays and angles are generated based on the parameters from Table III and channel coefficients are created using the same antenna model. The evaluation procedure is repeated for these channel coefficients to confirm that the resulting parameters are similar to the ones in Table III.

IV. RESULTS AND DISCUSSION

The fitted parameters for the eight LSPs are shown in Table III, together with the resimulation results for the dense urban and rural scenarios. The inter-parameter correlation values of the random variables X in (26) are given in Table IV. The upper right part (shown in white) contains the values for the LOS channels, the lower left part shows the values for the NLOS channels. Our simplified propagation model doses not consider polarization effects which need detailed information about the materials and incidence angles. Hence, we reuse the XPR values from [1] and fit the results to (26). In the following, the results are discussed:

Path loss (PL): In [1], the NLOS-PL is modeled by the FSPL and additional clutter loss, which models the attenuation caused by buildings and objects on the ground. We used this model for the NLOS parameters in Table III. Depending on the scenario, the elevation angle and the frequency, the NLOS-PL is about 15 to 45 dB higher compared to the FSPL. This leads to very low received NLOS power, e.g. in urban or dense urban scenarios where the clutter loss is highest. When adding a LOS component (assuming that the NLOS power does not change), it dominates the overall PL formula since it has about 30 to 3000 times more power compared to the scattered signals from buildings and vegetation. This is also the case in [1] where the LOS-PL is the same as the FSPL. In the resimulation, the parameterized model is able to create similar values. However, there is a slight increase in the frequency-dependence PL_γ which is compensated by a slightly lower base value PL_μ.

Shadow fading (SF): SF occurs when an obstacle gets positioned between the satellite and the MT. This leads to a reduction in signal strength because the wave is shadowed or blocked by the obstacle. We used the NLOS-SF model parameters from [1] to model the power fluctuations of the scattered paths. However, the power of the LOS component is deterministic. Hence, the LOS-SF is much smaller compared to the NLOS-SF because only the scattered paths can vary in strength. This is the case in our results in Table III. However, [1] reports significantly larger LOS-SF of 4 dB for the urban and dense urban scenarios. Partial shadowing of the first Fresnel zone might cause fluctuations of the LOS path strength which increases the SF.

TABLE III
LARGE-SCALE PARAMETERS FOR SATELLITE CHANNEL MODELS

Parameter	Unit		Dense Urban		Urban		Suburban		Rural		Dense Urb. Resim.		Rural Resim.	
			LOS	NLOS	LOS	NLOS	LOS	NLOS	LOS	NLOS	LOS	NLOS	LOS	NLOS
No. clusters	N/A	L	11	10	11	10	9	8	7	6	31	30	19	18
PL	dB	PL_μ	32.45	54.9	32.45	54.9	32.45	47.5	32.45	47.5	31.1	52.65	31.05	47.95
PL dist. dep.	dB / $\log_{10}$m	PL_ϵ	20.0	20.0	20.0	20.0	20.0	20.0	20.0	20.0	20.05	20.2	20.0	19.7
PL freq. dep.	dB / $\log_{10}$GHz	PL_γ	20.0	27.9	20.0	27.9	20.0	22.8	20.0	22.8	20.95	29.6	20.95	24.2
PL elevation dep.	dB / $\log_{10}$rad	PL_α	0	−11.0	0	−11.0	0	−8.4	0	−8.4	−1.2	−11.05	−1.3	−9.6
Shadow Fading	dB	SF_σ	0.15	10.0	0.1	6.0	1.45	10.4	1.4	10.1	0.15	10.2	1.4	9.6
SF freq. dep.	dB / $\log_{10}$GHz	SF_δ	0	2.5	0	0	0	0.75	0	1.1	0	2.4	0	1.45
SF elev. dep.	dB / $\log_{10}$rad	SF_β	−0.6	−2.5	0	0	0.85	1.25	1.0	1.3	−0.85	−2.55	0.7	0.75
SF decorr. dist.	m	SF_λ	50.0	50.0	50.0	50.0	50.0	50.0	50.0	120.0	N/A	N/A	N/A	N/A
KF	db	KF_μ	22.45	N/A	22.45	N/A	13.95	N/A	15.0	N/A	21.75	N/A	14.35	N/A
KF freq. dep.	db / $\log_{10}$GHz	KF_γ	7.9	N/A	7.9	N/A	2.8	N/A	2.8	N/A	8.15	N/A	3.25	N/A
KF elevation dep.	db / $\log_{10}$rad	KF_α	−11.0	N/A	−11.0	N/A	−8.4	N/A	−8.3	N/A	−11.85	N/A	−8.75	N/A
KF STD	db	KF_σ	10.6	N/A	5.65	N/A	11.05	N/A	9.85	N/A	10.65	N/A	9.55	N/A
KF STD freq. dep.	db / $\log_{10}$GHz	KF_δ	2.2	N/A	0	N/A	0	N/A	1.15	N/A	2.2	N/A	1.4	N/A
KF STD elev. dep.	db / $\log_{10}$rad	KF_β	−2.65	N/A	0	N/A	1.3	N/A	1.4	N/A	−3.05	N/A	1.05	N/A
KF decorr. dist.	m	KF_λ	50.0	N/A	50.0	N/A	50.0	N/A	50.0	N/A	N/A	N/A	N/A	N/A
DS	$\log_{10}$s	DS_μ	−7.95	−6.95	−7.8	−6.85	−7.45	−6.7	−6.85	−6.1	−7.9	−6.95	−6.85	−6.1
DS freq. dep.	$\log_{10}$s / $\log_{10}$GHz	DS_γ	−0.4	0	−0.4	0	0	0	0	0	−0.4	0	0	0
DS elevation dep.	$\log_{10}$s / $\log_{10}$rad	DS_α	0.4	0	0.5	0	0.35	0	0.35	0	0.45	0	0.35	0
DS STD	$\log_{10}$s	DS_σ	0.7	0.15	0.3	0.15	0.5	0.15	0.5	0.2	0.7	0.15	0.5	0.2
Delay Factor	N/A	r_{DS}	2.5	2.3	2.0	2.3	2.3	2.3	3.8	1.7	N/A	N/A	N/A	N/A
Clst. DS	ns	cDS_μ	4.95	4.95	4.95	4.95	4.95	4.95	4.95	4.95	N/A	N/A	N/A	N/A
Clst. DS freq. dep.	ns / $\log_{10}$GHz	cDS_γ	−2.2	−2.2	−2.2	−2.2	−2.2	−2.2	−2.2	−2.2	N/A	N/A	N/A	N/A
DS decorr. dist.	m	DS_λ	50.0	40.0	50.0	40.0	50.0	40.0	50.0	36.0	N/A	N/A	N/A	N/A
ASA	$\log_{10}°$	ASA_μ	0.9	1.9	0.9	1.9	1.15	1.9	1.1	1.85	0.8	1.85	1.1	1.8
ASA freq. dep.	$\log_{10}°$ / $\log_{10}$GHz	ASA_γ	−0.4	0	−0.4	0	0	0	0	0	−0.4	0	−0.1	0
ASA elevation dep.	$\log_{10}°$ / $\log_{10}$rad	ASA_α	0.55	0	0.5	0	0.4	0	0.4	0	0.65	0	0.45	0
ASA STD	$\log_{10}°$	ASA_σ	0.7	0.1	0.3	0.1	0.5	0.1	0.5	0.1	0.7	0.05	0.5	0.1
Cluster ASA	°	$cASA$	3.0	3.0	3.0	3.0	3.0	3.0	3.0	3.0	N/A	N/A	N/A	N/A
ASA decorr. dist.	m	ASA_λ	50.0	50.0	50.0	50.0	50.0	50.0	50.0	40.0	N/A	N/A	N/A	N/A
ESA	$\log_{10}°$	ESA_μ	0.3	1.25	0.45	1.0	0.85	0.4	0.8	−0.4	0.55	1.25	0.8	0.1
ESA freq. dep.	$\log_{10}°$ / $\log_{10}$GHz	ESA_γ	−0.4	0	−0.4	0	0	0	0	0	−0.4	0	0	0
ESA elevation dep.	$\log_{10}°$ / $\log_{10}$rad	ESA_α	0.7	0	1.15	0	1.4	0	1.4	0	1.0	0	1.25	0
ESA STD	$\log_{10}°$	ESA_σ	0.7	0.15	0.3	0.25	0.5	0.4	0.5	0.5	0.7	0.15	0.5	0.2
Cluster ESA	°	$cESA$	1.0	1.0	1.0	1.0	1.0	1.0	1.0	1.0	N/A	N/A	N/A	N/A
ESA decorr. dist.	m	ESA_λ	50.0	50.0	50.0	50.0	50.0	50.0	50.0	50.0	N/A	N/A	N/A	N/A
ASD	$\log_{10}°$	ASD_μ	1.85	2.9	1.95	3.05	2.25	3.20	2.9	3.75	1.75	2.95	3.0	3.85
ASD dist. dep.	$\log_{10}°$ / $\log_{10}$m	ASD_ϵ	−1.0	−1.0	−1.0	−1.0	−1.0	−1.0	−1.0	−0.95	−0.95	−1.0	−1.0	−0.95
ASD freq. dep.	$\log_{10}°$ / $\log_{10}$GHz	ASD_γ	−0.4	0	−0.4	0	0	0	0	0	−0.45	0	0	0
ASD elevation dep.	$\log_{10}°$ / $\log_{10}$rad	ASD_α	0.3	−0.25	0.85	−0.25	0	−0.25	0	−0.25	0.35	−0.25	0	−0.25
ASD STD	$\log_{10}°$	ASD_σ	0.7	0.25	0.35	0.2	0.55	0.2	0.55	0.25	0.7	0.25	0.5	0.3
ASD decorr. dist.	m	ASD_λ	50.0	50.0	50.0	50.0	50.0	50.0	50.0	30.0	N/A	N/A	N/A	N/A
ESD	$\log_{10}°$	ESD_μ	1.75	2.85	1.8	2.95	2.15	3.1	2.85	3.7	1.7	2.90	2.9	3.75
ESD dist. dep.	$\log_{10}°$ / $\log_{10}$m	ESD_ϵ	−1.0	−1.0	−1.0	−1.0	−0.95	−1.0	−1.0	−1.0	−1.0	−1.0	−1.0	−1.0
ESD freq. dep.	$\log_{10}°$ / $\log_{10}$GHz	ESD_γ	−0.4	0	−0.4	0	0	0	0	0	−0.4	0	0	0
ESD elevation dep.	$\log_{10}°$ / $\log_{10}$rad	ESD_α	0.5	0	0.85	0.5	1.05	0.65	1.05	0.65	0.5	0	1.1	0.65
ESD STD	$\log_{10}°$	ESD_σ	0.7	0.15	0.35	0.2	0.55	0.2	0.55	0.2	0.7	0.15	0.55	0.25
ESD decorr. dist.	m	ESD_λ	50.0	50.0	50.0	50.0	50.0	50.0	50.0	50.0	N/A	N/A	N/A	N/A
XPR	db	XPR_μ	15.15	15.15	7.0	7.0	12.65	12.65	7.0	7.0	14.75	14.4	7.0	7.05
XPR elevation dep.	db / $\log_{10}$rad	XPR_α	−13.45	−13.45	0	0	−11.2	−11.2	0	0	−13.5	−14.2	0	0
XPR STD	db	XPR_σ	13.65	13.65	3.0	3.0	10.95	10.95	3.0	3.0	13.55	12.7	3.0	2.95
XPR STD el. dep.	db / $\log_{10}$rad	XPR_β	8.8	8.85	0	0	2.7	2.7	0	0	9.45	9.25	0	0
XPR decorr. dist.	m	XPR_λ	50.0	50.0	50.0	50.0	50.0	50.0	50.0	40.0	N/A	N/A	N/A	N/A

Ricean K-factor (KF): The KF is the ratio between the power of the direct path and the power of scattered paths. It is only defined for LOS scenarios. Due to our characterization method, the KF in Table III reflects the difference between the NLOS-PL and the FSPL. Values can range up to 40 dB in the urban and dense urban scenarios at low elevation in the KA-band. The values reported in [1] are consistent with our findings only for the urban and the rural scenario. The dense urban and the suburban show show much lower KF results, especially at low elevation angles. It is unclear where this inconsistency comes from.

Delay spread (DS): The DS is an important measure for the delay time extent of a multipath radio channel. It is defined as the square root of the second central moment of the power-delay profile. The NLOS-DS is consistent with the distance to the scatterers in Table II. The dense urban scenario has an average value of 112 ns. This value increases with decreasing building density to 794 ns in the rural scenario. There is no frequency or elevation dependence in our model, since local scattering does not depend on the satellite position. In contrary, values reported in [1] show a decreasing DS for increasing α in the three urban scenarios and increasing DS for the rural

TABLE IV
INTER-PARAMETER CORRELATION VALUES

Inter-Parameter Correlations		L O S						
		DS	KF	SF	ASD	ASA	ESD	ESA
DS	Dense Urban	1	−0.8	0.2	0.8	0.8	0.8	0.8
	Urban	1	−0.8	0.1	0.8	0.8	0.8	0.8
	Suburban	1	−0.8	0.4	0.8	0.8	0.8	0.8
	Rural	1	−0.8	0.4	0.8	0.8	0.8	0.8
KF	Dense Urban	0	1	−0.3	−0.8	−0.8	−0.8	−0.8
	Urban	−0.1	1	−0.1	−0.8	−0.8	−0.8	−0.8
	Suburban	0	1	−0.6	−0.8	−0.8	−0.8	−0.8
	Rural	0	1	−0.5	−0.8	−0.8	−0.8	−0.8
SF	Dense Urban	0	N/A	1	0.2	0.2	0.2	0.2
	Urban	0	N/A	1	0.1	0.1	0.1	0.1
	Suburban	0	N/A	1	0.5	0.5	0.5	0.4
	Rural	−0.1	N/A	1	0.5	0.5	0.4	0.4
ASD	Dense Urban	0.2	N/A	0	1	0.8	0.8	0.8
	Urban	0.2	N/A	0	1	0.8	0.8	0.7
	Suburban	0.2	N/A	0	1	0.8	0.8	0.8
	Rural	0.2	N/A	0	1	0.8	0.8	0.8
ASA	Dense Urb.	0.1	N/A	0	0.1	1	0.8	0.8
	Urban	0.1	N/A	0	0.1	1	0.8	0.8
	Suburban	0.1	N/A	0	0.1	1	0.8	0.8
	Rural	0.2	N/A	0	0.2	1	0.8	0.8
ESD	Dense Urb.	0.1	N/A	0	0.3	0.1	1	0.8
	Urban	0.4	N/A	0	0.4	0.1	1	0.8
	Suburban	0.5	N/A	0	0.3	0.2	1	0.8
	Rural	0.5	N/A	0	0.3	0.2	1	0.8
ESA	Dense Urb.	−0.1	N/A	0	−0.1	0	0	1
	Urban	−0.1	N/A	0	−0.2	0	−0.1	1
	Suburban	−0.1	N/A	0	−0.2	0	−0.2	1
	Rural	0	N/A	0	−0.2	0	−0.2	1

(N L O S labels along the left edge of the table)

scenario. The reported values are much smaller at 41 ns in the dense urban scenario and 11 ns for the rural scenario ($\alpha = 50°$, $f = 20$ GHz). This would mean that in the rural scenario, the average distance between the MT and the scattering objects is only about 3 m compared to the 240 m in our model. When a LOS component is added to the existing NLOS model, the DS decreases since most power is now allocated to the direct path. The LOS-DS parameters in Table II also inherit the frequency and elevation dependence from the KF and there is a strong negative correlation between the LOS-DS and the KF in Table IV. These strong correlations are not reported by [1] and the effect of the KF on the DS is not as strong. The resimulation results show an almost perfect match with the initial parameters. However, the per-cluster DS introduced by [1] effectively splits each cluster into three sub-clusters which tipples the number of clusters in the resimulation output.

Azimuth spread of arrival (ASA): In our model, the ASA was drawn from a Uniform distribution in the range $[-\pi, \pi[$. Given that the scattered paths have similar power values, the average NLOS-ASA for 10 clusters is 84°. This value is achieved consistently for all scenarios in our model. However, values in [1] indicate much smaller NLOS-ASAs of around 30° for the dense urban scenario and 3-6° for the other scenarios. At the same time, [1] proposes a large per-cluster ASA of up to 30° and a small number of 2-4 clusters. Defining an AS for only 2 clusters while at the same time having a large AS within the clusters seems unreasonable. There is also no description of the clustering method nor an explanation and discussion of the results, making it hard

to interpret the findings. As for the DS, the ASA decreases when a LOS component is added. A frequency and elevation dependence of the LOS-ASA can also be observed due to the negative correlation with the KF.

Elevation spread of arrival (ESA): Since the average building height decreases in our model when moving from a dense urban to a rural scenario, the NLOS-ESA decreases as well from around 18° to well below 1°. When we add a LOS component, the ESA values decrease for the Urban and increase for the Rural scenarios. The scattered paths always arrive from the horizontal plane. Hence, there is an increasing difference in the elevations components between the NLOS paths and the direct path. This increases the ESA when the satellite is high up in the sky. All values reported in [1] have a strong elevation-dependency. This intuitively makes sense for the LOS channels where the direct path has a strong influence on the ESA. However, there is no explanation for the NLOS channels. For example, in the Rural-NLOS scenario, the ESA changes from 0.1° when the satellite is at the horizon to 22° when it is at the zenith. Calculating scatterer positions from those angles places them several kilometer up in the air which make no sense in a Rural setting with mostly low buildings. Also, [1] reports a strong frequency-dependence in the suburban case where at $\alpha = 50°$ the S-band ESA is 0.01° and the KA-band value is 24°. This is not reported for the other scenarios.

Azimuth spread of departure (ASD) and elevation spread of departure (ESD): The departure-ASs plays an important role in multi-beam satellite systems. The model parameters must reflect the multipath environment on the ground. Too large values might cause interference in neighboring beams. However, the beam centers are often separated by several hundred kilometers on the ground, outside the range of scattered paths. Since the satellite can be in different orbit heights, ASD and ESD must depend on the distance between the satellite and the terminal. This is the case for the values in Table III, where the departure-ASs decrease with increasing distance. It is not considered by [1]. In addition to the distance-dependence, there is a dependence on the satellite elevation angle. The ESD is smallest when the satellite is just above the horizon and increases when it moves to the zenith. This is also not reported by [1].

V. CONCLUSIONS

In this paper, we proposed a non-geostationary-satellite motion model which has been integrated into the open-source quasi deterministic radio channel generator (QuaDRiGa) channel model. We also proposed a simplified method to obtain the model parameters and we were able to produce a consistent set of parameters for four typical environments. Our parameter-set also produces almost identical calibration results as the parameter-set provided by 3GPP [2][1]. This is mainly due to the fact, the calibration was done for LOS channels only which

[1]The calibration was done using QuaDRiGa v2.4. The source code and the results are available at [3]

are dominated by the direct path. However, our method does not include many important radio propagation effects such as diffraction, polarization or interactions with different kinds of materials. It is therefore important to use measurements or ray-tracing methods to refine these parameters in the future.

REFERENCES

[1] 3GPP TR 38.811 v15.2.0, "Study on new radio (NR) to support non terrestrial networks," Tech. Rep., 09 2018.

[2] 3GPP TR 38.821 v16.0.0, "Solutions for nr to support non-terrestrial networks (ntn)," Tech. Rep., 12 2020.

[3] [Online]. Available: https://www.quadriga-channel-model.de

[4] 3GPP TR 38.901 v16.1.0, "Study on channel model for frequencies from 0.5 to 100 GHz," Tech. Rep., 2019.

[5] S. Jaeckel, L. Raschkowski, F. Burkhardt, and L. Thiele, "A spatially consistent geometric D2D small-scale fading model for multiple frequencies," *Proc. IEEE VTC Fall '19*, 2019. [Online]. Available: http://arxiv.org/abs/1906.12149

[6] ——, "Efficient sum-of-sinusoids based spatial consistency for the 3gpp new-radio channel model," *Proc. IEEE Globecom Workshops '18*, 2018.

[7] E. Eberlein, F. Burkhardt, G. Sommerkorn, S. Jaeckel, and R. Prieto-Cerdeira, "MIMOSA - analysis of the MIMO channel for LMS systems," *Space Communications*, vol. 22, no. 2-4, pp. 145–158, 2013.

[8] F. Burkhardt, E. Eberlein, S. Jaeckel, G. Sommerkorn, and R. Prieto-Cerdeira, "MIMOSA–a dual approach to detailed land mobile satellite channel modeling," *International Journal of Satellite Communications and Networking*, 2014.

[9] ITU-R S.1503-3, "Functional description to be used in developing software tools for determining conformity of non-geostationary-satellite orbit fixed-satellite service systems or networks with limits contained in article 22 of the radio regulations," Tech. Rep., 01 2018.

[10] S. Jaeckel, "Quasi-deterministic channel modeling and experimental validation in cooperative and massive MIMO deployment topologies," Ph.D. dissertation, TU Ilmenau, 2017. [Online]. Available: https://www.db-thueringen.de/receive/dbt_mods_00032895